Orm1 protects steatotic livers against ischaemia-reperfusion injury by stabilising Prdx1 and activating the Pi3k/Akt axis

YUMING WANG[1,2*], RUIDONG DING[1,2*], HAILUN CAI[3*], HUAN LIU[1,2], YILIN WANG[1,2], XIANGHENG CAI[1,2] and JINZHEN CAI[1,2]

[1]Organ Transplantation Centre, Affiliated Hospital of Qingdao University, Qingdao, Shandong 266100, P.R. China; [2]Institute of Organ Donation and Transplantation, Medical College of Qingdao University, Qingdao, Shandong 266100, P.R. China; [3]Department of Hepatopancreaticobiliary Surgery, Henan Provincial People's Hospital, Zhengzhou University, Zhengzhou, Henan 450000, P.R. China

Received June 25, 2026; Accepted September 24, 2026

DOI: 10.3892/ijmm.2026.6042

Abstract. The clinical utilization of steatotic donor livers is constrained by their marked sensitivity to ischemia/reperfusion (I/R) injury. In the present, Orosomucoid 1 (Orm1) was identify as a pivotal endogenous guardian against steatosis-associated hepatic I/R damage. Transcriptomic profiling of steatotic livers following I/R identified 1,551 differentially expressed genes, revealing a significant induction of Orm1. Functionally, adenovirus-mediated knockdown of Orm1 in high-fat diet fed mice markedly exacerbated I/R-induced liver injury, evidenced by significant elevations in serum ALT and AST (>2-fold increase), along with increased hepatocellular necrosis and apoptosis. Conversely, Orm1 overexpression in a palmitic acid and oleic acid-induced steatotic hepatocyte model effectively reduced reactive oxygen species production and rescued cells from hypoxia/reoxygenation-induced death (improving viability by 35%). Mechanistically, RNA-sequencing analysis of Orm1-knockdown livers identified 3,327 differentially expressed genes highly enriched in the PI3K/Akt pathway. Integrated immunoprecipitation-mass spectrometry and Co-immunoprecipitation assays demonstrated that Orm1 interacts with Peroxiredoxin 1 (Prdx1). In addition, it was demonstrated that Orm1 functions as a molecular stabilizer of Prdx1 by protecting it from ubiquitin-proteasomal degradation, which in turn sustains the activation of the PI3K/Akt survival axis. Pharmacological blockade of Prdx1 or inhibition of Akt significantly reversed Orm1-mediated hepatoprotection. In conclusion, the present findings delineate the Orm1-Prdx1-PI3K/Akt axis as a novel regulatory mechanism in steatotic liver I/R injury, providing a promising mechanistic basis for future therapeutic development.

Correspondence to: Dr Jinzhen Cai or Dr Xiangheng Cai, Organ Transplantation Centre, Affiliated Hospital of Qingdao University, 16 Jiangsu Road, Qingdao, Shandong 266100, P.R. China
E-mail: caijinzhen@qdu.edu.cn
E-mail: xiangheng1994@126.com

*Contributed equally

Key words: ischaemia-reperfusion, steatotic liver, transplantation, Orm1

Introduction

Liver transplantation remains the definitive therapeutic intervention for acute liver failure, end-stage liver disease and advanced hepatocellular carcinoma. However, the growing demand for transplantation is constrained by an acute shortage of donor organs (1,2). Driven by the global escalation of obesity and metabolic syndrome, the prevalence of metabolic dysfunction-associated steatotic liver disease (MASLD) has increased, leading to a steady increase in the proportion of steatotic 'marginal' donor livers (grafts outside ideal criteria that remain usable after risk assessment) (3,4). Steatosis sensitizes the hepatic parenchyma to ischemia/reperfusion (I/R), markedly reducing graft tolerance and increasing the risk of early graft dysfunction or primary nonfunction post-transplantation (5). While innovative strategies, including new preservation solutions and machine perfusion techniques, have been explored to mitigate damage to steatotic livers (6,7), their widespread clinical implementation remains restricted by logistical and technical barriers (8,9). Thus, elucidating the molecular mechanisms governing I/R injury in the context of steatosis is imperative for developing targeted interventions to optimize graft quality and expand the donor pool.

Activation of apoptosis, a markedly regulated form of programmed cell death essential for maintaining tissue homeostasis, plays a central role in the pathogenesis of hepatic I/R injury (10-12). Notably, steatotic livers exhibit a notably heightened apoptotic response during I/R, yet the precise regulatory networks and the specific reasons why steatosis exacerbates this process remain poorly understood (6). Apoptosis is orchestrated by a complex interplay of extrinsic and intrinsic signals, both of which converge on the activation of the Caspase protease family (13,14). Specifically, the executioner caspase-3/7 is activated by the upstream initiators caspase-8 and caspase-9 (15). The intrinsic pathway is governed primarily by the BCL-2 family, which dictates mitochondrial

outer membrane permeabilization and the subsequent release of cytochrome c to trigger the caspase-9 cascade (16-18). Despite these fundamental insights, the specific molecular switches that sensitize steatotic livers to I/R-induced apoptosis have yet to be fully identified.

Orosomucoid 1 (Orm1), also known as α1-acid glycoprotein, has emerged as a potential candidate for modulating hepatic resilience. Orm1 is a prominent acute-phase protein synthesized predominantly by the liver, although it can be induced in various extrahepatic tissues (19,20). It exerts pleiotropic biological functions, ranging from immune modulation and capillary barrier maintenance to the regulation of sphingolipid metabolism and the neutralization of reactive oxygen species (ROS) (21). Orm1 promotes NF-κB-mediated inflammation in chronic kidney transplant rejection (22) and serves as a marker of psoriasis and sepsis-related neuroinflammation (23,24); however, its role in acute hepatic I/R injury under metabolic stress remains unclear. Therefore, the present study aimed to investigate the role of Orm1 in steatotic liver I/R injury and to elucidate the underlying Orm1-Prdx1-Akt regulatory mechanism.

In the current study, it was demonstrated that Orm1 expression is significantly upregulated in response to steatotic liver I/R injury. Functionally, Orm1 deficiency exacerbates hepatic damage, whereas Orm1 overexpression confers protection against hypoxia-induced death in steatotic hepatocytes. Mechanistically, it was revealed that Orm1 directly interacts with and stabilises the peroxiredoxin 1 (Prdx1) protein by shielding it from ubiquitination-mediated degradation. This stabilisation subsequently sustains the activation of the Pi3k/Akt survival signalling pathway, ultimately inhibiting apoptosis. Collectively, the present findings uncovered a novel Orm1-Prdx1-Akt regulatory axis that safeguards steatotic livers from I/R injury, providing a promising theoretical foundation for optimizing the utilisation of 'marginal' graft and improving transplantation outcomes.

Materials and methods

Animals and study approval. C57BL/6 mice (Beijing Huafukang Biotechnology Co., Ltd.) were housed under a standard 12 h light/dark cycle with *ad libitum* access to food and water. The mice were fed a high-fat diet (HFD, 60% fat) for 12 weeks to induce hepatic steatosis. All animal protocols were approved by the Animal Ethics Committee of Qingdao University (approval no. 20260401C57BL/6452026 0601066) and conducted in accordance with NIH guidelines (publication no. 88-23, revised 1996).

Cell culture and treatment. AML12 cells (The Cell Bank of Type Culture Collection of The Chinese Academy of Sciences; https://www.cellbank.org.cn/search-detail.php?id=893) were cultured in RPMI 1640 medium (GUMD-B303; HyCyte™; Suzhou Haixing Biotechnology Co., Ltd.) supplemented with 10% foetal bovine serum (FCP-X310; HyCyte™; Suzhou Haixing Biotechnology Co., Ltd.) and 1% penicillin-streptomycin at 37˚C in a humidified 5% CO_2 atmosphere. To establish an *in vitro* MASLD model, AML12 cells were treated with a 750 μM free fatty acid mixture composed of palmitic acid (PA; 12 mM) and oleic acid (OA; 12 mM) at a 1:2 molar ratio at 37˚C for 24 h. This specific concentration and OA-enriched ratio was selected based on a previously established protocol to robustly induce hepatic lipid accumulation while minimising lipotoxicity (25).

For hypoxia/reoxygenation (H/R) experiments, the cells were subjected to 6 h of hypoxia (37˚C, 1% O_2, 5% CO_2) in a gas-controlled incubator, followed by standard 12 h of reoxygenation (37˚C, 21% O_2, 5% CO_2) for the indicated durations.

Drug treatments. HY-149394 (cat. no. HY-149394), HY-10249A (cat. no. HY-10249A), HY-18749 (cat. no. HY-18749), MG132 (cat. no. HY-13259) and chloroquine (CQ; cat. no. HY-17589A) were all purchased from MedChemExpress. For *in vitro* experiments (cell H/R experiments), cells were treated with HY-149394 (50 μM), HY-10249A (5 μM), HY-18749 (10 μM), MG132 (20 μM) or CQ (50 μM) for 10 h at 37˚C. In the H/R model, these compounds were added at the onset of reoxygenation (following 6 h of hypoxia) and maintained throughout the 12 h reoxygenation period. For *in vivo* experiments, mice were administered HY-149394 (10 mg/kg), HY-10249A (55 mg/kg) or HY-18749 (10 mg/kg) via intraperitoneal injection at 1 h prior to the induction of ischaemia.

Oil Red O staining. For lipid accumulation analysis, cells cultured in confocal dishes or tissue sections were washed with PBS and fixed with 4% paraformaldehyde for 30 min at room temperature. After washing with PBS, the samples were stained with Oil Red O working solution (cat: BL941A; Biosharp Life Sciences) for 20 min at room temperature, followed by differentiation with 60% isopropanol for 5 sec. The samples were then washed with distilled water, counterstained with hematoxylin (cat: BL702B; Biosharp Life Sciences) for 10 min at room temperature and examined under a CKX53 cell culture microscope (Olympus Corporation).

Detection of ROS. The intracellular ROS level was determined using DCFH-DA (cat: S0033S, Beyotime Biotechnology). After overnight seeding of the cells, the cells were subjected to H/R treatment at 37˚C. Subsequently, the cells were washed with PBS and incubated with 10 μM DCFH-DA in serum-free medium at 37˚C in the dark for 20 min. After three washes with PBS, the fluorescence signal was detected by fluorescence microscopy.

Animal model. Male C57BL/6 mice (aged 8 weeks, weighing 22-25 g) were randomly allocated to experimental groups. Following an overnight fast (~12 h) with *ad libitum* access to water, the mice were anaesthetised via intraperitoneal injection of pentobarbital sodium (50 mg/kg). Subcutaneous injection of buprenorphine (0.1 mg/kg) was administered for postoperative analgesia. During the surgical procedure, core body temperature was continuously monitored and maintained at 37˚C using a feedback-controlled heating pad.

A standard 70% hepatic I/R model was established. After midline laparotomy, systemic heparinisation was achieved via intravenous injection of heparin (100 U/kg). The blood supply to the left and median liver lobes was occluded using an atraumatic microvascular clamp. Successful occlusion was immediately confirmed by visual blanching (pale discolouration) of the targeted liver lobes.

After 60 min of ischaemia, the clamp was removed to initiate reperfusion, which was confirmed by the restoration of colour in the ischaemic lobes. Sham-operated mice underwent identical surgical procedures, including laparotomy and vessel dissection, but without vascular occlusion. The 6 h reperfusion time points were selected based on preliminary experiments and previous literature (25), establishing these time points as the peak of acute liver injury and inflammatory responses in this model.

At the end of the designated reperfusion period (6 h), mice were euthanized with an intraperitoneal overdose of pentobarbital (150 mg/kg) for collection of blood and liver tissue samples. To minimize potential bias, all subsequent histological and biochemical assessments were performed by investigators blinded to the experimental groups.

Intravenous adenoviral injection and treatment. Mice were intravenously injected via the tail vein with 100 μl of recombinant adenovirus encoding Orm1 (the adenovirus delivers shRNA targeting Orm1) ($1.0x10^{12}$ viral particles/ml (GIMRA Genomics; Shanghai GenePharma Co., Ltd.) or an equal volume of empty control adenovirus (NC). At 3 days postinjection, the mice were subjected to the aforementioned hepatic I/R procedure. shRNA primers can be found in Table SI.

In vitro hepatocyte transfection. The overexpression plasmid (100 μg/μl, GIMRA Genomics; Shanghai GenePharma Co., Ltd.) and transfection reagent (Lipofectamine™ 3000; Invitrogen; Thermo Fisher Scientific, Inc.) were mixed and incubated at room temperature for 15 min. The mixture was then added dropwise to the cultured cells and incubated at 37˚C for 48 h (Table SI). The mixture was then added dropwise to the cultured cells and incubated at 37˚C for 48 h (Table SI), after which the cells were harvested and subjected to subsequent experiments.

Liver function. Serum levels of alanine aminotransferase (ALT), aspartate aminotransferase (AST) were measured using an automatic chemistry analyser (AU5800; Olympus Corporation) and serum concentrations of triglyceride (TG) was determined using the TG assay kit (cat. no. A110; Nanjing Jiancheng Bioengineering Institute).

Immunohistochemical staining. Liver tissue samples were fixed in 4% paraformaldehyde at room temperature for 48 h and then embedded in paraffin for immunohistochemical analysis. Following deparaffinisation in xylene and rehydration through a graded series of ethanol (100, 95, 80, and 70%), antigen retrieval was carried out by heating the sections in citrate buffer (pH 6.0) at 95˚C for 20 min, the tissue sections were blocked and permeabilised with a solution containing 3% bovine serum albumin (cat. no. IA0910; Beijing Solarbio Science & Technology Co., Ltd.) at room temperature for 2 h and 0.4% Triton X-100 (cat. no. T8200; Beijing Solarbio Science & Technology Co., Ltd.) at room temperature for 1 h. The sections were then incubated with the corresponding primary antibodies (Orm1; 1:100; cat. no. 16439-1-AP; Proteintech Group, Inc.) overnight (12 h) at 4˚C, followed by incubation (2 h) at room temperature with the appropriate secondary antibodies (Anti-rabbit IgG H+L; 1:5,000; cat. no. RGAM009; Proteintech Group, Inc.). Antibody details can be found in Table SII.

Cellular immunofluorescence. At room temperature, AML12 cells cultured in confocal dishes were fixed with 4% paraformaldehyde (30 min), permeabilised with 0.1% Triton X-100 (2 h) and blocked with 5% goat serum (30 min) (cat: BL1097A; Biosharp Life Sciences) for immunofluorescence analysis. Following an overnight incubation with specific primary antibodies for Orm1 (1:400; cat. no. 16439-1-AP; Proteintech Group, Inc.) and Prdx1 (1:200; cat. no. 15816-1-AP; Proteintech Group, Inc.) at 4˚C, the cells were then labelled with Alexa Fluor 488-(1:100; cat no. SA00013-2; Proteintech Group, Inc.) and 594-(1:100; cat. no. SA00013-3; Proteintech Group, Inc.) conjugated secondary antibodies at room temperature for 2 h and counterstained with DAPI (cat no. 28718-90-3; Beijing Solarbio Science & Technology Co., Ltd.) at room temperature for 10 min. Images were acquired using a Leica STELLARIS 5 (Leica Microsystems GmbH) confocal laser scanning microscope. Antibody details can be found in Table SII.

PI/Hoechst staining assay. Hoechst/PI staining was performed to assess cell apoptosis and necrosis. AML12 cells were seeded in 12-well plates and subjected to the indicated treatments. The staining was performed according to the manufacturer's protocol (cat. no. C1056; Beyotime Biotechnology), and images were captured using a fluorescence microscope.

Transcriptome RNA sequencing (RNA-seq). Total RNA was extracted from frozen samples and cultured cells using TRIzol reagent (cat. no. 15596018; Invitrogen; Thermo Fisher Scientific, Inc.) according to the manufacturer's protocol (n=3 per group). RNA quality was assessed using a NanoDrop 2000 spectrophotometer (Thermo Fisher Scientific, Inc.), 1% agarose gel electrophoresis and an Agilent 5300 Fragment Analyzer (Agilent Technologies, Inc.) to determine RIN/RQN values; only samples with ≥1 μg total RNA, ≥30 ng/μl concentration, RQN >6.5 and OD260/280 of 1.8-2.2 were used. Library construction and paired-end (PE150) sequencing were performed by Shanghai Majorbio Bio-Pharm Technology Co., Ltd. using an Illumina NovaSeq 6000 platform with a NovaSeq 6000 SP reagent kit (100 cycles; cat. no. 2002746; Illumina, Inc.), with the final library loaded at 1-20 pM as quantified by Qubit 4.0 and Agilent 5300 (Agilent Technologies, Inc.). Differentially expressed genes (DEGs) were identified using the DESeq2 package (version 1.36.0; https://bioconductor.org/packages/DESeq2/) in R software (version 4.2.1; RStudio, Inc.), with significance thresholds of $|\log_2$ fold change$|>1$ and adjusted P-value (false discovery rate) <0.05. Kyoto encyclopaedia of genes and genomes (KEGG; https://www.kegg.jp/kegg/pathway.html) pathway enrichment analysis was performed using the Majorbio Cloud Platform (Shanghai Majorbio Bio-Pharm Technology Co., Ltd.; https://cloud.majorbio.com)

Silver staining. Gels were silver-stained using a Fast Silver Stain Kit (cat. no. P0017S; Beyotime Biotechnology) according to the manufacturer's instructions. Briefly, gels were fixed (50% ethanol/10% acetic acid, 20 min at room temperature), washed

with 30% ethanol (10 min at room temperature) and Milli-Q water (10 min at room temperature), sensitized (2 min at room temperature), stained with 1x silver solution (10 min at room temperature) and developed until protein bands were visible at room temperature. The reaction was stopped, and gels were washed and stored in Milli-Q water at room temperature.

Coimmunoprecipitation (Co-IP) and mass spectrometry. Cells were lysed using NP-40 lysis buffer (cat. no. P0013F; Beyotime Biotechnology). For immunoprecipitation, the lysates were incubated overnight at 4˚C with specific antibodies for Orm1 (1:50; cat. no. 16439-1-AP; Proteintech Group, Inc.) or control IgG (1:50; cat. no. A7028, Beyotime Biotechnology). Protein A/G magnetic beads (20 μl; cat. no. P1791; Beyotime Biotechnology) were then added to the lysates and incubated for an additional 2 h at room temperature with gentle rotation. After extensive washing, bead-bound immunocomplexes were resolved by SDS-PAGE, and the subsequent immunoblotting procedure was performed as described in the 'Western blot analysis' section. Gel bands of interest were excised and sent to Shanghai Majorbio Bio-Pharm Technology Co., Ltd. for LC-MS/MS analysis. Samples were reduced with 10 mM TCEP (37˚C, 60 min), alkylated with 40 mM IAM (room temperature, 40 min in the dark), precipitated with acetone and digested with trypsin (1:40, m/m) at 37˚C overnight. Peptides were desalted on a C18 column and quantified with a NanoDrop One (cat: 840-317400, Thermo Fisher Scientific, Inc.). A total of 400 ng of peptides was loaded onto the column for each LC-MS/MS run. Liquid chromatography-mass spectrometry was performed on a Vanquish Neo HPLC system (Thermo Fisher Scientific, Inc.) coupled to a timsTOF HT mass spectrometer (Bruker Corporation) with Compass HyStar software (Bruker Corporation). Separation was conducted on a homemade column (15 cm x100 μm, 1.7 μm) over 8 min at a flow rate of 300 nl/min using mobile phases A (2% acetonitrile/0.1% formic acid) and B (80% acetonitrile/0.1% formic acid). Data were acquired in positive ionisation mode with a capillary voltage of 1.6 kV, a nitrogen drying gas temperature of 180°C, an ion mobility range of 0.7-1.3 V·sec/cm^2, and a mass scan range of 300-1,500 m/z in data-independent acquisition mode. As Co-IP magnetic bead samples were used, no additional quality control was performed prior to mass spectrometry.

Western blot analysis. Total protein was extracted using RIPA lysis buffer (Beyotime Biotechnology). Protein concentration was determined using a BCA protein assay kit (cat. no. PC0020; Beijing Solarbio Science & Technology Co., Ltd.) according to the manufacturer's instructions. Following quantification, the protein concentrations were adjusted accordingly, and equal amounts of protein (20 μg per lane) were loaded into SDS-polyacrylamide gels with varying concentrations (8%, 10% or 12%). These gel samples were subsequently subjected to electrophoresis, and the proteins obtained were then transferred onto polyvinylidene fluoride membranes. The membrane was incubated with specific primary antibodies overnight at 4˚C, followed by incubation with appropriate horseradish peroxidase (HRP)-conjugated secondary antibodies (1:50,000; cat no. HA1023; HUABIO) for 2 h at room temperature. The primary antibodies used in the present study included anti-Orm1 (1:5,000; cat. 16439-1-AP; Proteintech Group, Inc.), anti-Bcl2 (1:1,000; cat. no. 3498 T; Cell Signaling Technology), anti-Bax (1:1,000; cat. no. 2772 T; Cell Signaling Technology), anti-Pi3k (1:1,000; cat. no. HA722522; HUABIO), anti-Akt (1:2,000; cat. no. HA721870; HUABIO), anti-P-Pi3k (1:2,000; cat. no. HA721673; HUABIO), anti-P-Akt (1:1,000; cat. no. HA724447; HUABIO) and anti-β-actin (1:5,000; cat. no. AB0035; Abways) antibodies. The protein bands were visualised using an enhanced chemiluminescence detection system (Tanon Science and Technology Co., Ltd.). The details of relevant antibodies are presented in Table SII.

RNA extraction and reverse transcription-quantitative PCR (RT-qPCR). Total RNA was extracted using an RNA rapid extraction kit (Suzhou Xinsaimei Biotechnology Co., Ltd.) according to the manufacturer's instructions. Reverse transcription was performed using a PrimeScript RT kit (cat. no. 639505; Takara Bio, Inc.) according to the manufacturer's instructions. Briefly, genomic DNA was removed by incubation with gDNA Eraser at 42˚C for 2 min, followed by reverse transcription at 37˚C for 15 min and inactivation at 85˚C for 5 sec. RT-qPCR was performed using TransStart® Green qPCR SuperMix UDG (cat. no. AQ111; TransGen Biotech Co., Ltd.), which contains SYBR Green I as the fluorescent dye. Each 20 μl reaction mixture contained 10 μl of 2x TransStart® Green qPCR SuperMix UDG, 0.4 μl of forward primer (10 μM), 0.4 μl of reverse primer (10 μM), 0.4 μl of Passive Reference Dye (50x; added according to the qPCR instrument used), an appropriate amount of template and nuclease-free water to a final volume of 20 μl. The thermocycling conditions were as follows: 50˚C for 2 min (UDG incubation), 94˚C for 10 min (UDG inactivation), followed by 40-45 cycles of 94˚C for 5 sec, 60˚C for 15 sec and 72˚C for 10 sec, followed by a dissociation stage. Fluorescence signals were acquired during the annealing or extension step, with acquisition times adjusted according to the manufacturer's instructions for the specific instrument. β-actin (Proteintech Group, Inc.) was used as the endogenous control gene. Relative gene expression was calculated using the $2^{-\Delta\Delta Cq}$ method (26). The relevant primers are detailed in Table SIII.

Cell Counting Kit (CCK)-8 assay. A CCK-8 was obtained from Suzhou Xinsaimei Biotechnology Co., Ltd. AML12 cells were seeded into 96-well plates at a density of 1x10^4 cells per well and cultured in complete medium for 12 h. Following the indicated treatments and H/R exposure, 10 μl of CCK-8 solution was added to each well. After the cells were incubated for an additional 2 h at 37˚C, the absorbance at 450 nm was measured using a microplate reader.

TUNEL staining. Liver tissues were fixed in 4% paraformaldehyde for 1 h at room temperature, embedded in paraffin and cut into 5-μm-thick sections. Following standard deparaffinisation and rehydration, the sections were permeabilised with proteinase K (20 μg/ml) for 20 min at 37˚C and washed twice with PBS. TUNEL staining was performed using a TUNEL apoptosis detection kit (cat. no. G4890; Beijing Solarbio Science & Technology Co., Ltd.) according to the manufacturer's instructions. Briefly, sections were incubated with 50 μl of TUNEL reaction mixture containing TdT

enzyme and FITC-labelled dUTP at 37˚C for 60 min in the dark. After washing with PBS, nuclei were counterstained with DAPI (10 μg/ml) for 5-10 min at room temperature in the dark. Sections were then mounted with an anti-fade mounting medium and images were captured using a fluorescence microscope (Olympus Corporation) with excitation at 450-500 nm and emission at 515-565 nm.

Cycloheximide (CHX) chase assay. To assess protein stability, cells were treated with the protein synthesis inhibitor CHX (50 μM; cat. no. HY-12320; MedChemExpress) for the indicated durations (37˚C; 0, 2, 4 and 8 h). After treatment, the cells were collected and lysed in RIPA buffer supplemented with protease inhibitors. The lysates were sonicated and centrifuged at 12,000 x g, for 15 min at 4˚C, and the resulting supernatants were collected. Protein samples were then mixed with loading buffer, denatured, resolved by SDS-PAGE, and analysed by western blotting (as aforementioned) using specific antibodies to evaluate protein expression levels over time.

Data acquisition. In the present study, the GSE193764 dataset was obtained from the Gene Expression Omnibus (GEO) database (https://www.ncbi.nlm.nih.gov/geo/query/acc.cgi?acc=GSE193764). This dataset includes 12 pretransplant and 12 posttransplant samples from rats with steatotic livers. Differential expression analysis was performed using R software (version 4.2.1; RStudio, Inc.). The resulting DEGs were subsequently validated using the GSE279693 dataset (7), where genes showing consistent expression trends with our dataset were considered validated. For single-cell RNA-seq data (CRA004061) (27), which were downloaded from the Genome Sequence Archive of the National Genomics Data Center (https://ngdc.cncb.ac.cn/gsa/), dimensionality reduction and gene-to-cell mapping analyses were conducted using Seurat v4 (https://satijalab.org/seurat/).

Statistics. Sample sizes for *in vivo* experiments (n=4 per group) were determined based on our preliminary studies and similar publications in the field to ensure adequate statistical power (28). The animals were randomly allocated to different experimental groups. To minimise bias, histological evaluations and signal quantifications were performed by investigators who were blinded to the group assignments. Preestablished exclusion criteria included surgical mortality before the designated endpoint/severe infection; no other data points or samples were excluded. All *in vitro* experiments were performed with at least three independent biological replicates, with specific replicate numbers detailed in the respective figure legends.

Statistical analysis and data visualisation were performed using GraphPad Prism (version 9.0; Dotmatics). Data are presented as the mean ± standard deviation (SD). Before applying the parametric tests, the assumption of normality was assessed using the Shapiro-Wilk test, and the homogeneity of variance was evaluated using the Brown-Forsythe test or Levene's test.

Comparisons between two independent groups were performed using an unpaired two-tailed Student's t test for normally distributed data with equal variances. Welch's t test was applied when the assumption of equal variance was violated, and the Mann-Whitney U test was used for non-normally distributed data. Experiments involving three or more groups (such as multiarm rescue experiments and inhibitor/agonist treatments), data were analysed using one-way analysis of variance (ANOVA) followed by Tukey's post hoc test. Two-way ANOVA followed by Bonferroni post hoc correction was employed to analyse data with two independent variables. The Kruskal-Wallis test followed by Dunn's post hoc test was utilised for non-parametric data across multiple groups.

Representative images were selected from independent experiments with results approximating the group mean. $P<0.05$ was considered to indicate a statistically significant difference.

Results

Orm1 expression is upregulated during I/R in steatotic livers. The rat transcriptomic dataset GSE193764 was analysed to identify key molecular drivers of I/R in steatotic livers. Differential expression analysis revealed 1,551 DEGs, including 1,112 upregulated and 439 downregulated genes (Table SIV). Notably, Orm1 emerged as a significantly upregulated candidate gene following transplantation (Figs. 1A and S1). To further validate these findings, the mouse dataset GSE279693 was examined, which confirmed a consistent and significant increase in Orm1 expression during I/R in steatotic livers (Fig. 1B). Given this marked upregulation, the cellular source of Orm1 was further investigated using the CRA004061 single-cell dataset. Dimensionality reduction and cluster analysis revealed that Orm1 was predominantly expressed in hepatocytes (Fig. 1C-F). This cell type specificity is consistent with the findings of previous reports identifying hepatocytes as the primary site of Orm1 synthesis (29).

To validate Orm1 expression, a mouse model of hepatic I/R in steatotic livers was employed (Fig. 2A). After 12 weeks of HFD feeding, H&E staining revealed moderate hepatic steatosis, characterised by the presence of lipid droplets (Fig. 2B), in line with prior reports (30). Serum and liver tissue TG levels were significantly greater in HFD-fed mice compared with normal diet-fed mice (Fig. 2C and D), and their body weights were also significantly greater (Fig. S2A).

HFD-fed mice were then subjected to 1 h of ischaemia followed by 6 h of reperfusion. Western blotting and RT-qPCR analysis demonstrated that I/R significantly upregulated Orm1 expression in steatotic liver tissues (Fig. 2E and F). Immunohistochemical analysis further confirmed elevated Orm1 levels after I/R, as reflected by increased immunohistochemical scores (Fig. 2G and H). In parallel, primary hepatocytes isolated from HFD-fed mice exhibited steatotic degeneration and were subjected to 6 h of hypoxia followed by 6 h of reoxygenation. Consistent with the aforementioned findings, both western blotting and RT-qPCR revealed a marked increase in Orm1 expression following H/R (Fig. S2B and C).

Collectively, these findings suggest that the upregulation of Orm1 expression represents an endogenous compensatory protective response to I/R in steatotic livers.

Orm1 knockdown in mice with diet-induced steatotic liver aggravated liver damage following I/R injury. Mice with

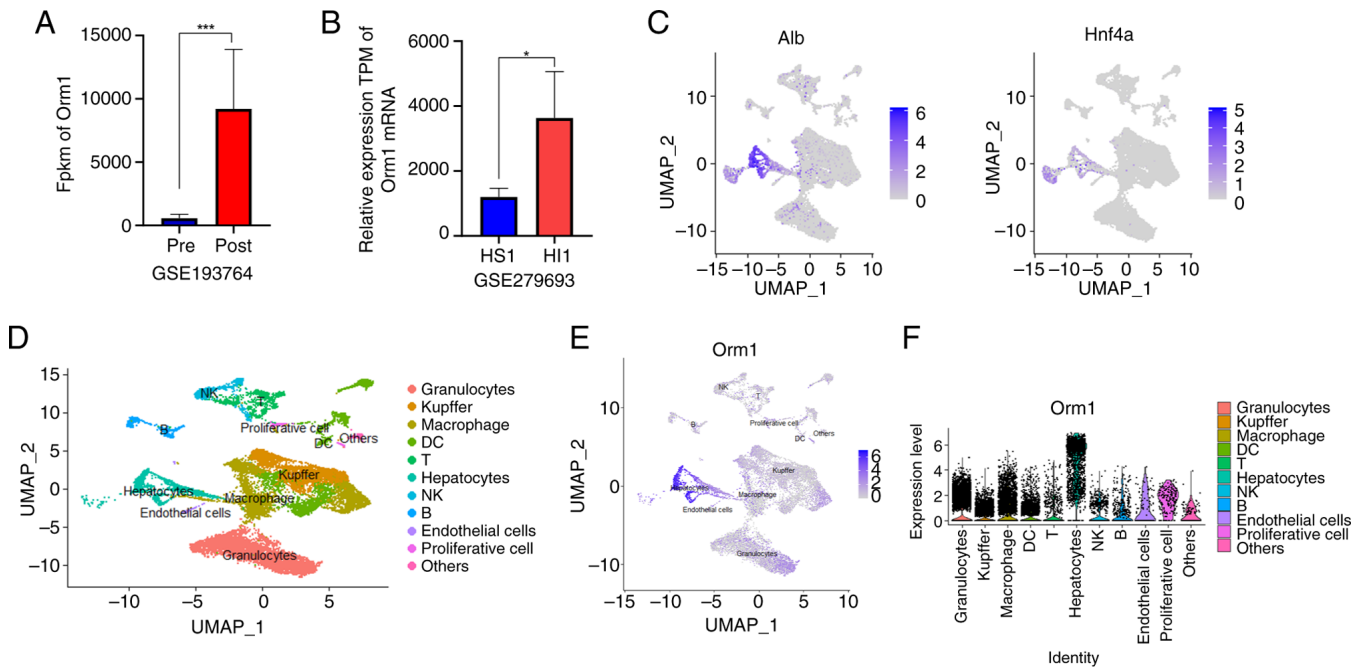


Figure 1. Expression of Orm1 in liver tissue. (A) Changes in *Orm1* mRNA levels in rats orthotopically transplanted with steatotic grafts from the GSE193764 dataset. (B) Changes in *Orm1* mRNA levels in mice with steatotic liver I/R in the GSE279693 dataset. (C and D) UMAP plot showing the composition of myeloid cells coloured by cluster and expression status of liver cell-specific markers. (E and F) The expression of Orm1 in different cell subpopulations. *P<0.05 and ***P<0.001.

specific Orm1 knockdown were generated using a recombinant adenovirus expressing shRNA targeting Orm1 (Adv-shOrm1). These mice were then subjected them to hepatic I/R to investigate the functional role of Orm1 in steatotic liver I/R (Fig. 3A). Western blotting and RT-qPCR confirmed that Orm1 expression was significantly lower in the liver tissues of Adv-shOrm1-treated mice than in those of control mice (Fig. 3B and C). Liver injury was assessed by measuring serum levels of AST and ALT, as well as by histologically evaluating of necrosis. Notably, Orm1 knockdown resulted in significantly elevated serum AST and ALT levels (Fig. 3D and E). Moreover, H&E staining revealed that the area of necrotic tissue was markedly larger in the Adv-shOrm1 group than in the Adv-shNC group (Fig. 3F). Given that apoptosis plays a critical role in the progression of hepatic I/R (31), the effect of Orm1 knockdown on hepatocyte apoptosis was further examined. TUNEL staining revealed a significant increase in the number of apoptotic cells in the livers of Adv-shOrm1 mice (Fig. 3G). Consistent with these findings, western blot analysis revealed that, compared with the control treatment, the knockdown of Orm1 led to upregulated expression of the pro-apoptotic protein Bax and downregulated expression of the anti-apoptotic protein Bcl-2 (Fig. 3H). These results indicate that Orm1 deficiency exacerbates liver injury and apoptosis following steatotic liver I/R.

Hepatocyte-specific Orm1 overexpression alleviated steatotic liver damage following I/R. An *in vitro* model of steatotic hepatocytes was established by treating AML12 cells with a PA:OA mixture to further clarify the functional role of Orm1 in hepatic I/R accompanied by steatosis. The oil red staining results revealed that the liver cells stimulated by the PA:OA mixture exhibited accumulation of lipids within the cells (Fig. S3A). Following successful modelling, an Orm1 overexpression plasmid was constructed to overexpress Orm1 in steatotic hepatocytes. Western blotting and RT-qPCR revealed that the expression of Orm1 was significantly increased in liver cells (Fig. S3B and C). Compared with the control, Orm1 overexpression significantly reduced the expression of the pro-apoptotic protein Bax and increased the expression of the anti-apoptotic protein Bcl-2 (Fig. S3D). Furthermore, overexpression of Orm1 markedly enhanced cell viability and decreased the number of PI-positive cells following H/R injury (Fig. S3E and F). These results suggest that Orm1 protects steatotic hepatocytes against apoptosis and cell death under ischaemic stress.

Orm1 regulated I/R in steatotic livers through the Pi3k/Akt pathway. RNA-seq was performed on liver tissues from Orm1 knockdown and wild-type mice following I/R to investigate the role of Orm1 in steatotic liver I/R. A total of 3,327 DEGs were identified, comprising 1,809 upregulated and 1,518 downregulated genes (Fig. 4A). KEGG pathway enrichment analysis revealed the top 20 signalling pathways ranked by P-value, among which the 'PI3K-Akt signalling pathway' was significantly enriched (Fig. 4B). Western blot analysis revealed that Orm1 knockdown markedly reduced the phosphorylation levels of Pi3k and Akt (Figs. 4C and S4A). Conversely, Orm1 overexpression in steatotic liver cells significantly increased phosphorylation levels of Pi3k and Akt (Figs. 4D and S4B).

The involvement of the Pi3k/Akt pathway was subsequently verified *in vivo* using mice treated with specific Adv-shOrm1. After 1 h of treatment with HY-18749 (an Akt agonist), the role of the Pi3k/Akt pathway was assessed in hepatic I/R induced by Orm1 knockdown in the steatotic liver. HY-18749 significantly reversed the detrimental effects of Orm1 knockdown following hepatic I/R (Fig. 5A-E). ALT and AST levels

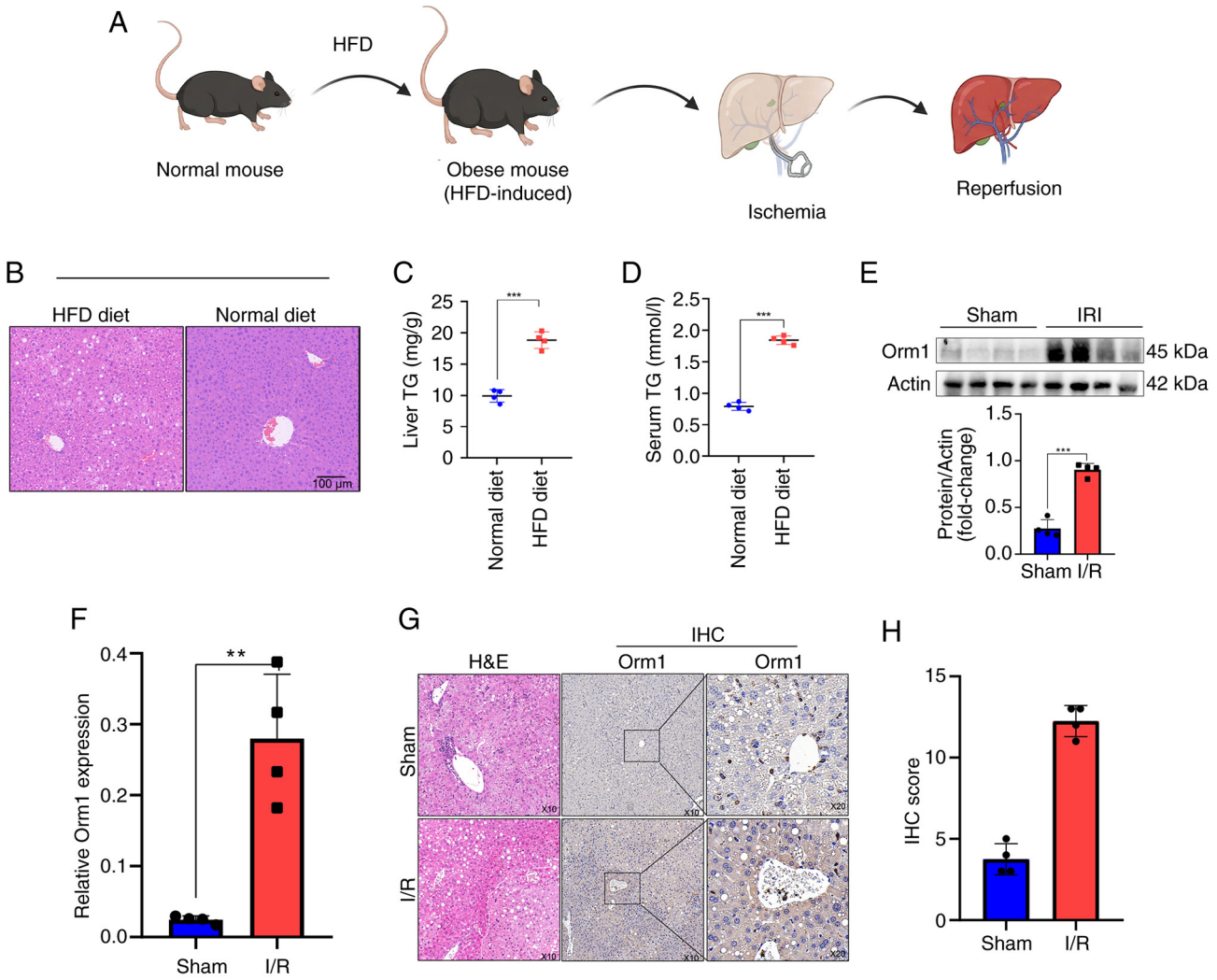


Figure 2. Orm1 expression is upregulated after I/R injury in steatotic livers. (A) Experimental design for I/R in steatotic livers. (B) Liver sections of mice that had been fed an HFD for 12 weeks were stained with H&E. (C and D) Serum and liver TG levels in the sham group and the HFD group (n=4/group). (E) Western blotting and (F) Reverse transcription-quantitative PCR analyses were used to measure Orm1 expression in mouse liver tissues from mice subjected to sham surgery or I/R (n=4/group). (G and H) Orm1 protein expression in the liver tissues of mice from the sham operation group and the I/R group, as determined by immunohistochemical analysis (n=4/group). **P<0.01 and ***P<0.001. I/R, ischaemia-reperfusion; HFD, high fed diet; IHC, immunohistochemistry; TG, triglyceride.

were significantly decreased (Fig. 5B and C), and the area of necrotic tissue was significantly reduced (Fig. 5D and E). Rescue experiments were performed using an Akt inhibitor (HY-10249A) to investigate the role of phosphorylated Pi3k and Akt in Orm1-mediated hepatic I/R in the steatotic liver. The results showed that treatment with an Akt inhibitor significantly aggravated liver injury, which was alleviated by Orm1 overexpression. CCK-8 and Hoechst/PI staining assays further revealed that, compared with the vector group, the Akt inhibitor markedly reduced the viability of steatotic liver cells (Fig. S5A and B). Hence, these findings suggest that Orm1 regulates hepatic I/R in the steatotic liver by modulating the activity of the Pi3k/Akt signalling pathway.

Orm1 interacted and colocalised with Prdx1. A combined immunoprecipitation-mass spectrometry (IP-MS) approach was used to identify novel Orm1-interacting proteins to further elucidate the mechanism by which Orm1 regulates Pi3k/Akt signalling. Prdx1 was ranked highest among the differentially enriched proteins associated with the Pi3k/Akt pathway when Orm1 antibody immunoprecipitates were compared with IgG controls (Fig. 5F and G and Table SV) (32,33). To validate the MS data, Co-IP assays were performed to confirm the physical interaction between Orm1 and Prdx1 (Fig. 5H). Additionally, confocal immunofluorescence microscopy revealed substantial colocalization of endogenous Orm1 and Prdx1 in AML12 cells (Fig. 5I). To further substantiate the physical interaction between Orm1 and Prdx1, an exogenous Co-IP assay was performed. Plasmids encoding Flag-tagged Orm1 (Flag-Orm1) and HA-tagged Prdx1 (HA-Prdx1) were co-transfected into cells. Subsequent immunoprecipitation using anti-Flag magnetic beads successfully co-precipitated HA-Prdx1. Notably, no HA signal was detected in the immunoprecipitates from the negative control cells transfected with HA-Prdx1 alone (Fig. S3G). This robust interaction between the exogenously tagged proteins, alongside the endogenous Co-IP and mass spectrometry data, validates the specific physical association between Orm1 and Prdx1.

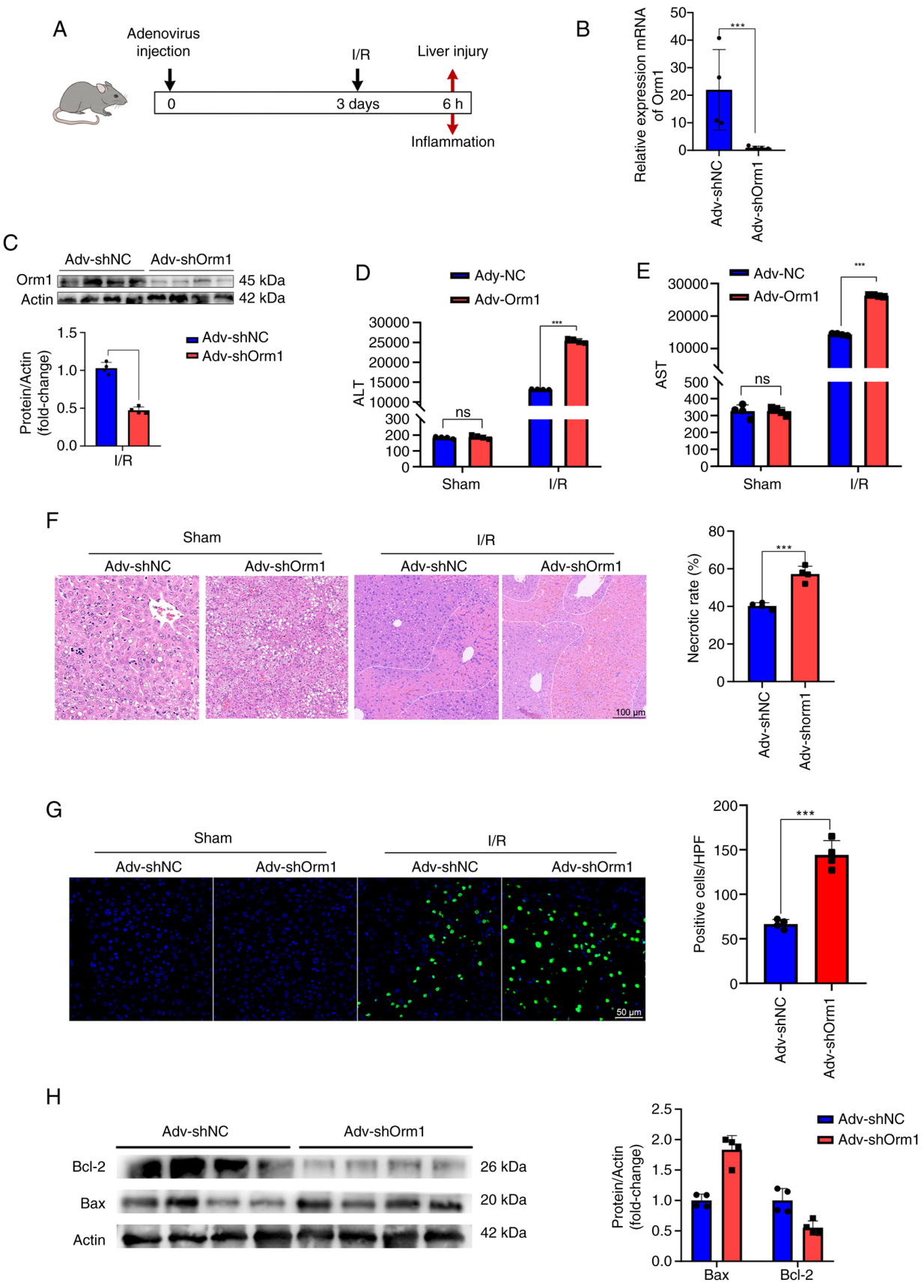


Figure 3. Knockdown of Orm1 aggravates I/R in steatotic livers. (A) Experimental design for Orm1 knockdown in mice. (B and C) Expression of Orm1 protein and RNA in the livers of the Adv-shNC group and Adv-shOrm1 group. (D and E) Serum ALT and AST levels in the livers of the NC and Orm1-KO mice with the steatosis group following the sham (n=4/group) and I/R surgery (n=4/group) groups. (F) Representative H&E-stained liver sections from the liver tissues of NC and Orm1-KO mice with steatotic livers following a sham operation and I/R injury (n=4/group). (G) TUNEL staining (green) and statistics for liver sections from NC and Orm1 mice following sham or I/R surgery (n=4/group). (H) Western blotting analysis of endogenous apoptosis-related protein expression in the steatotic liver subjected to I/R injury (n=4/group). ***P<0.001. I/R, ischaemia-reperfusion; ALT, alanine aminotransferase; AST, aspartate aminotransferase; shNC, non-coding short hair pin RNA; shOrm1, Omr1 short hair pin RNA; KO, knock out; ns, not significant.

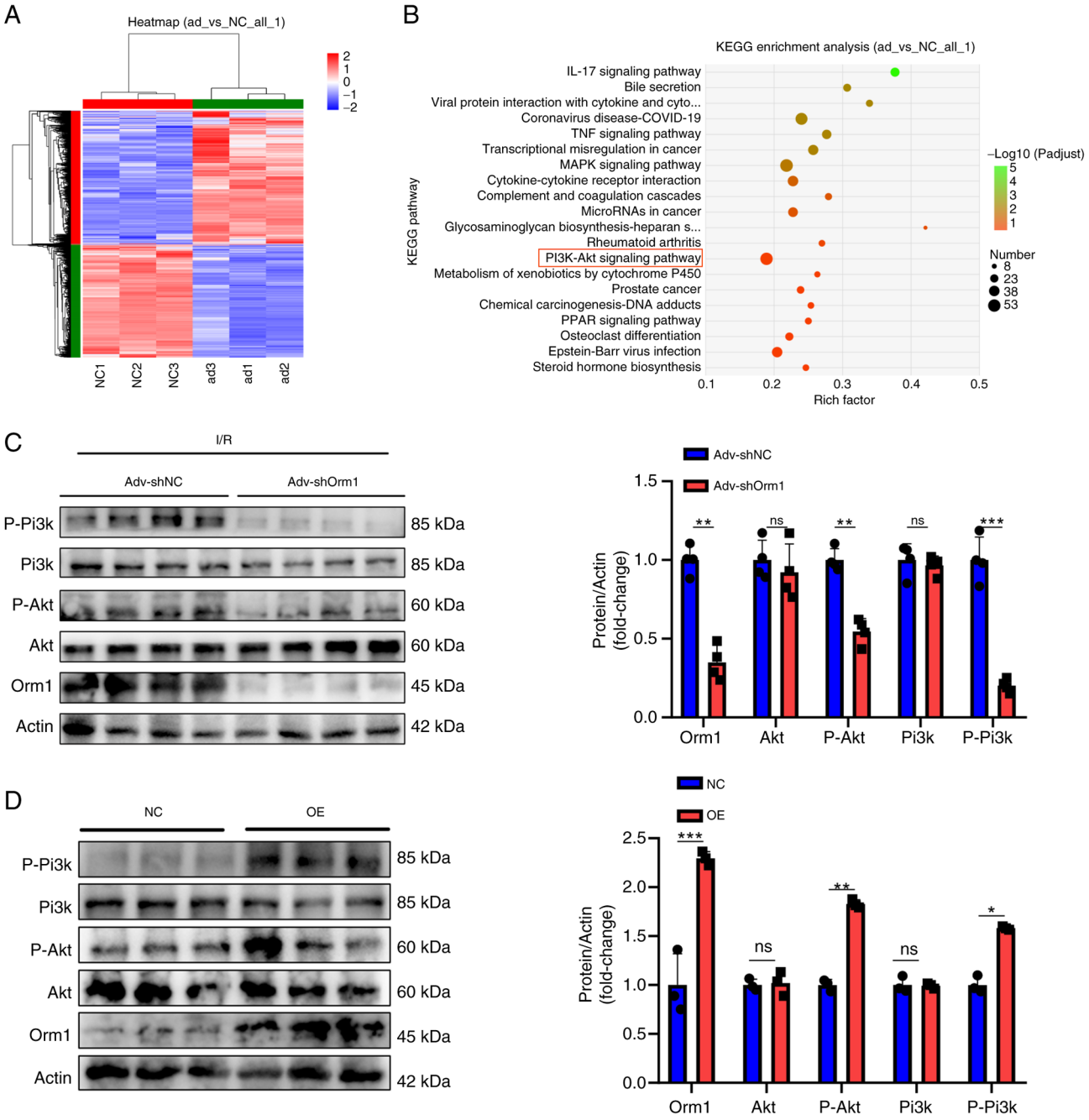


Figure 4. Orm1 participates in the Pi3k/Akt signalling pathway in steatotic hepatic I/R. (A) Heatmap of 3,327 differentially expressed genes identified by RNA-sequencing. (B) Top 20 signalling pathway maps enriched in the RNA-sequencing. (C and D) Western blotting was used to detect the protein expression levels of Orm1, p-Akt, Akt, p-Pi3k and Pi3k in mouse liver tissue following Orm1 knockdown and in fatty AML12 cells after Orm1 overexpression. *P<0.05, **P<0.01 and ***P<0.001. ns, not significant; I/R, ischaemia-reperfusion; shNC, non-coding short hair pin RNA; shOrm1, Omr1 short hair pin RNA; OE, overexpression.

Next, the cells were treated with the Prdx1-specific inhibitor HY-149394 to explore the functional role of Prdx1 in I/R. CCK-8 and Hoechst/PI staining revealed that, compared with DMSO treatment, Prdx1 inhibition significantly reduced hepatocyte viability and increased cell death (Fig. 6A and B). Furthermore, Prdx1 inhibition markedly suppressed the phosphorylation of Pi3k and Akt, upregulated the expression of the proapoptotic molecule Bax and downregulated the expression of the antiapoptotic protein Bcl-2 (Figs. 6C and S4C). Next, it was investigated whether altered Orm1 expression could concomitantly affect Prdx1 expression. Prdx1 protein levels were upregulated upon Orm1 overexpression and downregulated upon Orm1 knockdown (Fig. 6D and E); however, no significant changes were observed at the mRNA level (Fig. S5C), suggesting posttranscriptional or posttranslational regulation. These results indicate that Prdx1 activation protects hepatocytes against I/R through the Pi3k/Akt pathway and that Orm1 may regulate hepatocyte survival via the modulation of Prdx1 protein stability or activity.

Orm1 stabilised Prdx1 by inhibiting its ubiquitin proteasomal degradation. Previous studies have demonstrated that Prdx1 undergoes constitutive ubiquitination (34,35) and that

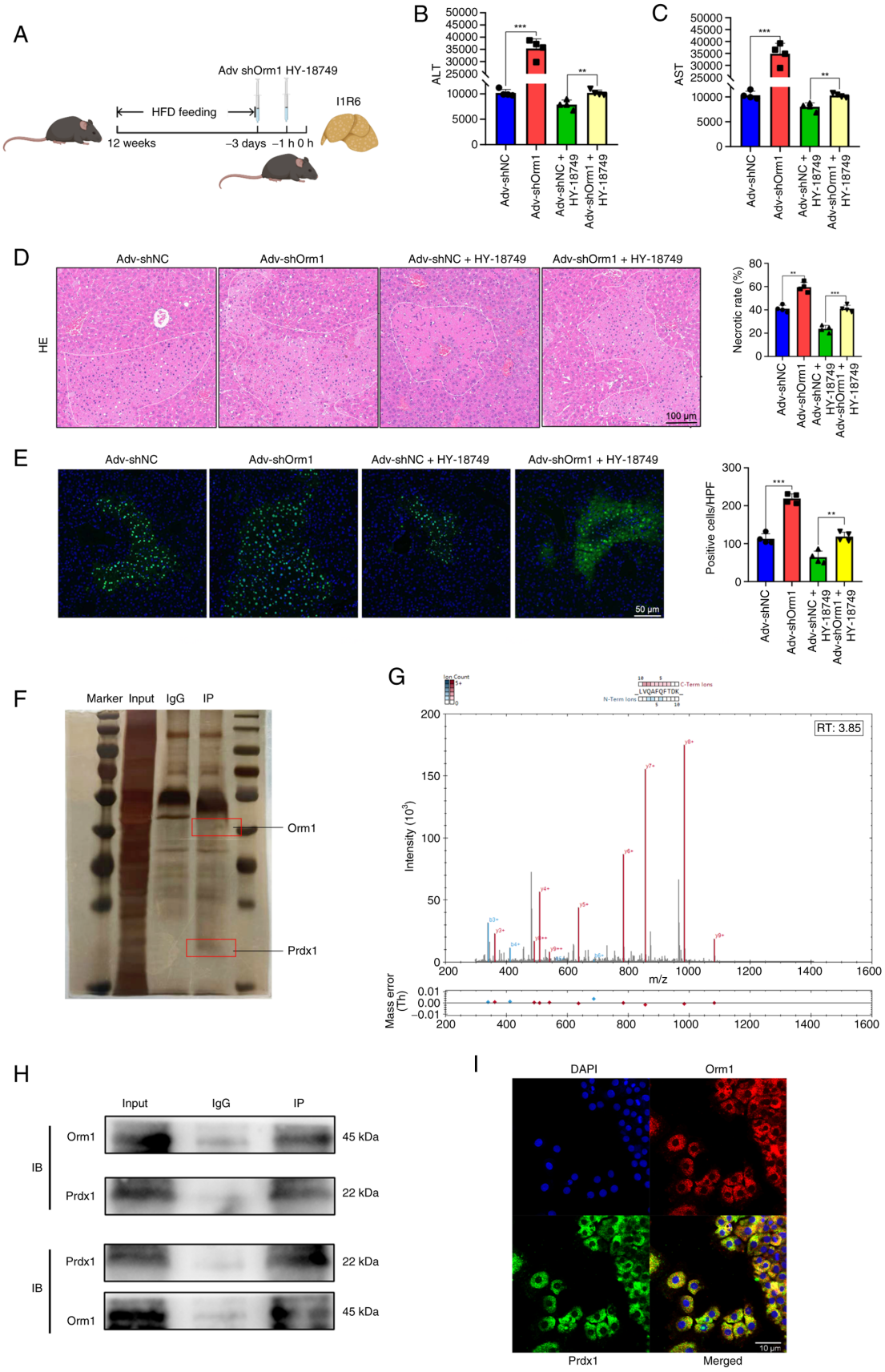


Figure 5. HY-18749 reverses the promoting effect of Orm1 knockdown on steatotic liver I/R. (A) Graphical representation of the experimental design: HY-18749, an AKT agonist, was administered intravenously 1 h before the ischaemia/reperfusion experiments in Orm1 gene-knockdown and control fatty liver mice. Serum (B) ALT and (C) AST levels in the indicated groups (n=4/group). (D) Representative H&E-stained liver sections from the indicated groups (n=4/group). (E) Representative TUNEL staining of liver sections (n=4/group). (F) The sensitive silver staining method was used to find the interacting proteins. (G) Mass spectrogram of Prdx1. (H) Co-IP analysis of Orm1 and Prdx1. (I) Confocal immunofluorescence analysis of Orm1 and Prdx1 expression. **P<0.01 and ***P<0.001. ALT, alanine aminotransferase; AST, aspartate aminotransferase; shNC, non-coding short hair pin RNA; shOrm1, Omr1 short hair pin RNA; IP, immunoprecipitation; IB, immunoblot.

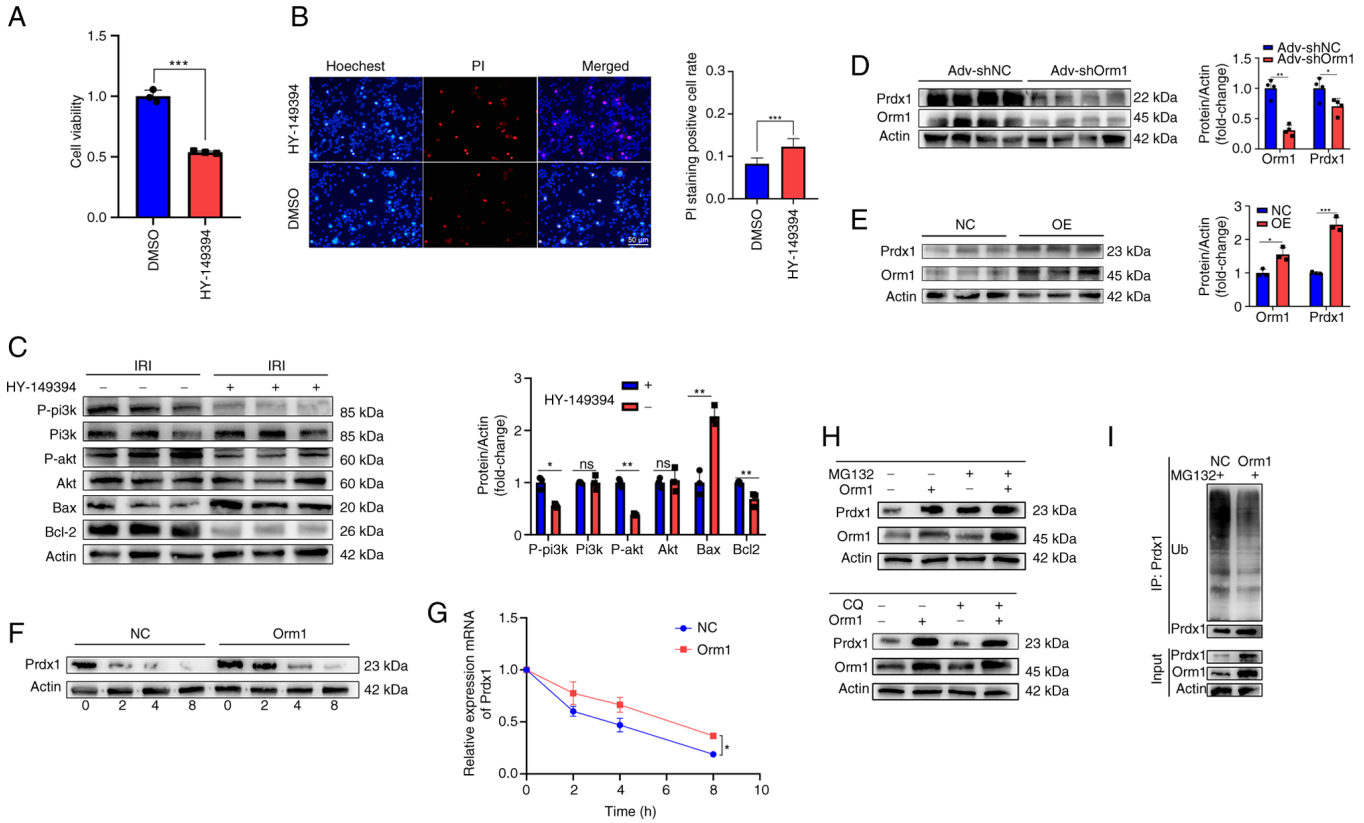


Figure 6. A Prdx1 inhibitor (HY-149394) decreases the viability of fatty liver cells. The results of the (A) cell counting kit-8 and (B) Hoechst/PI staining assay revealed that HY-149394 significantly exacerbated liver cell damage. (C) Western blotting analysis revealed that the Prdx1 inhibitor significantly inhibited the phosphorylation of Pi3k/Akt, decreased the expression level of Bcl-2, and increased the expression of Bax. (D and E) Western blot analysis revealed that the protein expression of Prdx1 was positively associated with that of Orm1 demonstrated using (D) knockdown or (E) OE of Orm1. (F and G) Control and Orm1-overexpressing AML12 cells were treated with CHX at different time points. (H) Orm1-overexpressing cells were treated with MG132 (20 μM) or CQ (50 μM) for 10 h, after which Prdx1 and Orm1 protein levels were determined by western blotting. (I) Ubiquitination assay. Orm1-overexpressing AML12 cells were treated with MG132 for 10 h, followed by immunoprecipitation with anti-Prdx1 and immunoblotting with the indicated antibodies. *P<0.05, **P<0.01 and ***P<0.001. ns, not significant; OE, overexpression; shNC, non-coding short hair pin RNA; shOrm1, Omr1 short hair pin RNA; IP, immunoprecipitation; IB, immunoblot.

endogenous protein degradation primarily occurs through the ubiquitin-proteasome and lysosomal pathways. CHX chase assays were performed to assess Prdx1 degradation dynamics. Orm1 overexpression significantly attenuated Prdx1 degradation in AML12 cells (Fig. 6F and G). To elucidate the degradation pathway, the cells were treated with the proteasome inhibitor MG132 or the lysosome inhibitor CQ. MG132 treatment restored Prdx1 levels in Orm1-knockdown cells, whereas CQ had no significant effect (Fig. 6H), indicating that Prdx1 is degraded primarily via the proteasomal pathway. Furthermore, cell-based ubiquitination assays revealed that Orm1 overexpression markedly reduced Prdx1 ubiquitination (Fig. 6I), suggesting that Orm1 protects Prdx1 from ubiquitin-mediated proteasomal degradation.

Orm1 regulated I/R in the steatotic liver via the Prdx1/Pi3k/Akt pathway. The role of Prdx1 in I/R of steatotic liver was further investigated. CCK-8 and Hoechst/PI staining assays revealed that the protective effect of Orm1 overexpression on hepatocyte injury was significantly reversed by a Prdx1 inhibitor (Fig. 7A and B), indicating that Prdx1 mediates the hepatoprotective effects of Orm1 in I/R. Subsequent *in vivo* experiments demonstrated that administration of an Akt agonist alleviated hepatic I/R induced by Prdx1 inhibition. Compared with the control group, which received the Akt agonist, the experimental group showed improved liver function (Fig. 7C and D). H&E staining revealed a reduction in the area of necrosis in the liver (Fig. 7E), along with a decrease in the proportion of TUNEL-positive cells (Fig. 7F). Overall, these findings indicate that overexpression of Orm1 alleviates hepatic I/R through the Prdx1-Pi3k-Akt axis. Prior to the subsequent experiments, the transfection efficiency of sh-Prdx1 was confirmed by RT-qPCR and western blotting (Fig. S5D and E). Furthermore, considering that oxidative stress is one of the core changes during cell and tissue H/R, the cells were subjected to H/R treatment. The results revealed that overexpression of Orm1 reduced the H/R-induced ROS production and (Figs. S6A-D) and that inhibition of Prdx1 expression reversed the protective effect of Orm1 overexpression (Fig. S6A-D). Subsequently, Prdx1-knockdown cells were treated with an AKT agonist, and the results revealed that the AKT agonist reversed the cell damage and ROS production caused by Prdx1 (Fig. S6A-D).

Discussion

Hepatic I/R is a key factor affecting the morbidity and mortality rates of liver resection and liver transplantation surgeries (36). In the present study, Orm1 was discovered as a

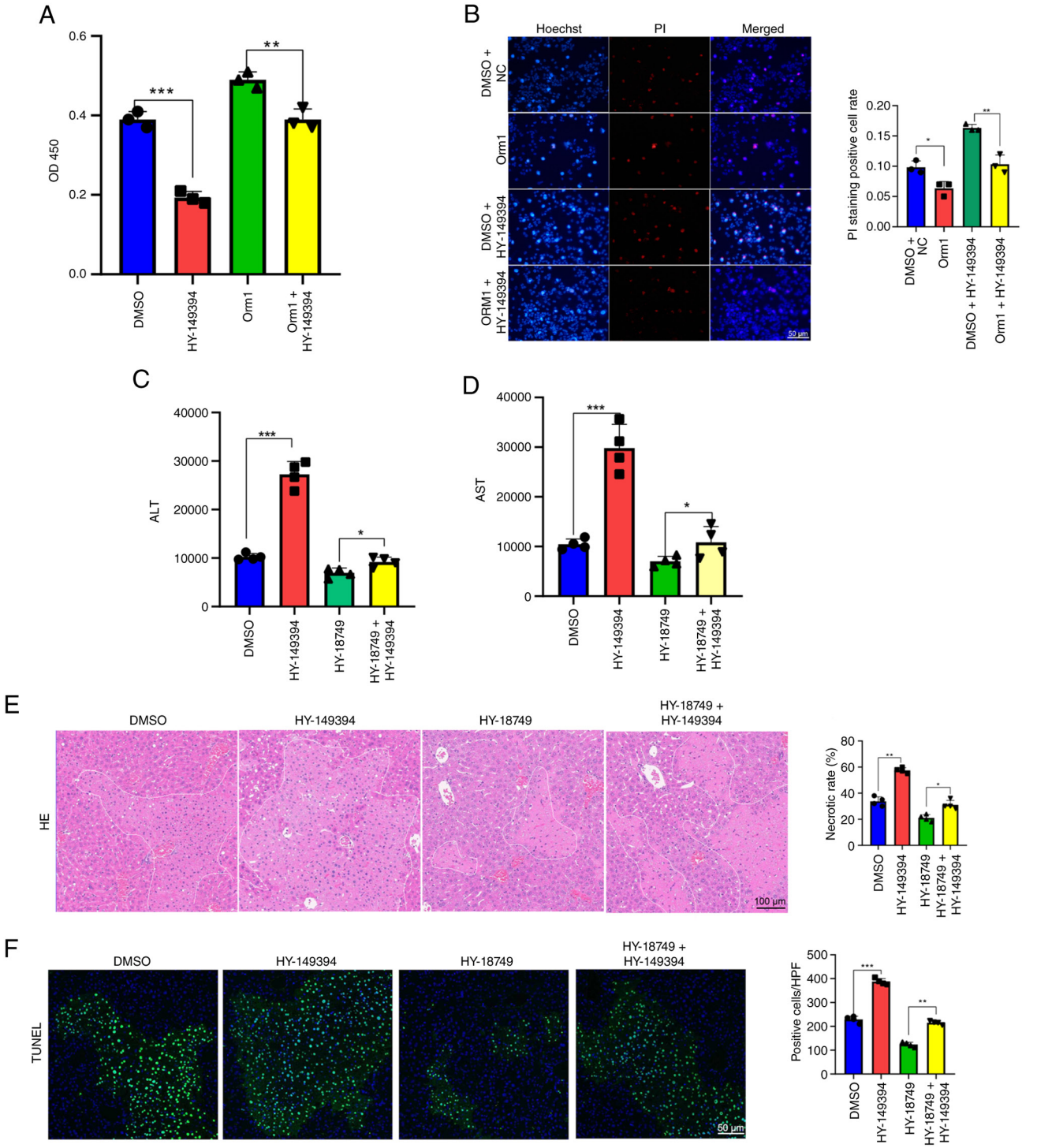


Figure 7. Orm1 exerts a protective effect on liver I/R in steatotic livers *in vivo* through the Prdx1/Pi3k/Akt pathway. The results of (A) the CCK-8 assay and (B) Hoechst/PI staining assay indicate that overexpression of Orm1 can alleviate hypoxia-induced damage in liver cells, and this protective effect can be reversed by the Prdx1 inhibitor HY-149394A. Serum (C) ALT and (D) AST levels in the indicated groups (n=4/group). (E) Representative H&E-stained liver sections from the indicated groups (n=4/group). (F) Representative TUNEL staining of liver sections (n=4/group). *P<0.05, **P<0.01 and ***P<0.001.

potential candidate molecule for treating I/R in the context of a steatotic liver. Although the current study primarily highlights the protective role of Orm1 in steatotic livers, its potential hepatoprotective effects in lean livers during I/R cannot be ruled out. The steatotic model was specifically focused on because 'marginal' steatotic grafts exhibit profound hypersensitivity to ischaemic and oxidative stress, making them more susceptible to primary non-function post-transplantation. Further studies comparing the differential dynamics of Orm1 expression between lean and steatotic livers will be valuable for determining whether this protective axis is uniquely amplified under metabolic stress. The results revealed that the expression of Orm1 in liver cells significantly increased after liver I/R and that inhibiting the expression of Orm1 aggravated liver injury, whereas overexpressing Orm1 had a protective effect on I/R. Mechanistic studies revealed that Orm1 interacted with

Prdx1, inhibiting its ubiquitination and degradation, thereby activating the Pi3k/Akt signalling pathway.

Orm1, also known as α1-acid glycoprotein, was first identified by Shimada and Schmidt more than a century ago (37). As a multifunctional acute-phase protein, Orm1 not only serves as a disease marker and drug carrier, but also participates in immune regulation, maintenance of capillary barrier function and sphingolipid metabolism. The corresponding receptors have been preliminarily identified in macrophages (CCR5), neutrophils (Siglec-5) and liver parenchymal cells (HBB) (29). Numerous studies have shown that Orm1 has a carcinogenic effect on various tumours. For instance, the absence of Orm1 can inhibit the proliferation, migration and invasion of renal clear cell carcinoma and induce apoptosis (19). Qiong and Yin (38) reported that Orm1 can promote the proliferation and migration of breast cancer cells, and its absence can downregulate the expression of transfer-related matrix metalloproteinases. In colorectal cancer and bladder cancer, Orm1 promotes tumour progression by promoting epithelial-mesenchymal transition and activating the ERK signalling pathway (39,40). Additionally, its role in non-tumour diseases has also been investigated. Studies have shown that Orm1 can improve temporomandibular joint osteoarthritis by maintaining cartilage homeostasis (41) and mediate LN-IgG podocyte injury and autophagy regulation through the AMPK/mTOR signalling pathway (20). In addition, Orm1 can alleviate doxorubicin-induced oxidative stress and apoptosis in cardiomyocytes through the Nrf2 signalling pathway (21). Furthermore, a recent study revealed that the Cebpa-Orm1 axis in liver cells can inhibit alcohol-related liver diseases (42). Classically, Orm1 is recognised as a secreted acute-phase glycoprotein involved in systemic inflammation (43), immunomodulation and drug binding; however, the present findings reveal an intracellular regulatory role for Orm1 during hepatic I/R. The present proposes that under stress, intracellular Orm1 directly regulates protein stability by physically shielding Prdx1 from ubiquitination. This mechanism preserves the cellular antioxidant capacity to counteract severe oxidative stress. In the present study, the expression of Orm1 in liver cells significantly increased after liver I/R; knockdown of Orm1 exacerbated liver injury, tissue necrosis and cell apoptosis, whereas overexpression of Orm1 exerted a protective effect.

This dual nature of Orm1, acting as an intracellular redox stabiliser and a secreted immunomodulator, has profound clinical implications for steatotic liver transplantation. In marginal grafts, early oxidative stress triggers apoptosis and activates innate immune pathways, exacerbating adverse transplant immunity (44). Therefore, rather than focusing on its broad role in tumours or other diseases, the present study specifically highlighted the Orm1-Prdx1 axis as a potential therapeutic target to mitigate oxidative injury and immune-mediated damage during liver transplantation.

The Pi3k/Akt signalling pathway plays a role in regulating cell apoptosis, and its phosphorylation activation can inhibit apoptosis (45-48). In tumour research, apigenin induces apoptosis and autophagy in liver cancer cells by inhibiting the Pi3k/Akt/mTOR pathway whereas, Adora2a promotes proliferation and inhibits apoptosis in colorectal cancer by activating the Pi3k/Akt pathway. By contrast, in a lipopolysaccharide-induced acute kidney injury model, rubiogenin alleviated inflammation and apoptosis by activating the Pi3k/Akt/Nrf2 pathway (47). To further investigate Orm1 in steatotic liver I/R, RNA-seq identified Prdx1 and Pi3k/Akt as key regulatory factors, and the function of the Orm1-Prdx1-Pi3k/Akt axis was further verified. The results of the functional rescue experiments revealed that Orm1 regulates Pi3k/Akt signalling through Prdx1, thereby affecting the apoptosis of steatotic liver cells. Compared with that in the control group, the protein level of Prdx1 increased after overexpression of Orm1, and the expression of apoptosis-related molecules in the Bcl-2 family significantly decreased; in a steatotic liver mouse model, inhibiting Orm1 led to a significant decrease in Prdx1 expression. Further mechanistic studies revealed that Orm1 interacts with Prdx1 to inhibit its ubiquitination and degradation, thereby activating the Pi3k/Akt signalling pathway and alleviating ischaemic injury to liver cells. The present study revealed the molecular mechanism underlying Orm1-mediated regulation of I/R in steatotic livers and expanded the understanding of its role in liver injury protection. The present study investigated the potential molecular mechanism of Orm1 in liver I/R. Ubiquitination, as an important posttranslational modification method, plays a role in protein stability and functional regulation. Previous studies have shown that Prdx1 can be regulated at the transcriptional and posttranscriptional levels and that its activity is also regulated by various modifications, such as ubiquitination, acetylation, phosphorylation, glutathionylation and S-nitrosylation (49,50). For instance, the E3 ligase HECTD3 can mediate the ubiquitination degradation of Prdx1 (51). The present study further confirmed that in steatotic liver cells, the absence of Orm1 can promote the degradation of Prdx1 via the ubiquitin-proteasome pathway.

Notably, although the present study initially revealed the mechanism of Orm1 in steatotic liver I/R, the I/R process involves a complex regulatory network of multiple factors and pathways, and numerous unanswered questions remain. For instance, whether Orm1 regulates apoptosis through other signalling pathways or participates in other biological processes remains unclear. Future studies are needed to comprehensively understand the function of Orm1 in steatotic liver I/R.

The present study initially revealed the protective mechanism of Orm1 in steatotic liver I/R; however, the I/R process involves a complex regulatory network of multiple factors and pathways, and several limitations remain to be addressed. First, although the present *in vitro* models demonstrate the cytoprotective effects of Orm1 overexpression against H/R injury, the present study lacks *in vivo* Orm1 overexpression models. However, a recent study demonstrated that *in vivo* restoration of ORM1 expression via AAV delivery or recombinant protein administration effectively rescues hepatic lipid accumulation in alcohol-associated liver disease (42). These *in vivo* findings are consistent with the present *in vitro* results and support the therapeutic potential of exogenous Orm1 administration, warranting future *in vivo* studies to validate its efficacy in optimizing steatotic liver grafts. Second, regarding the mechanism of Prdx1 stabilisation, a previous study demonstrated that another binding protein, IRAK1, can inhibit the ubiquitination of Prdx1 by blocking the activity of the E3 ubiquitin ligase HECTD3 (51). Given that Orm1 lacks intrinsic de-ubiquitinase activity, we hypothesise that the physical interaction between Orm1 and Prdx1 may occur through a similar mechanism,

causing steric hindrance. This spatial shielding may prevent specific E3 ubiquitin ligases, such as HECTD3, from accessing the ubiquitination sites on Prdx1. However, since this was not experimentally validated in the present the study this spatial shielding effect or the specific involvement of HECTD3, this mechanism remains strictly hypothetical. Further structural biology studies and targeted ubiquitination assays are needed to elucidate the precise interacting domains and to confirm this model. Finally, whether Orm1 regulates apoptosis through other signalling pathways or participates in other biological behaviours remains to be clarified. In summary, the present study revealed the protective effect of Orm1 in hepatic I/R. The molecular mechanism by which Orm1 interacts with Prdx1, inhibits the ubiquitination and degradation of Prdx1, and activates the Pi3k/Akt signalling pathway, thereby reducing hepatocyte apoptosis, has been elucidated. Targeting the Orm1-Prdx1-Pi3k/Akt axis is expected to become a potential therapeutic strategy for hepatic I/R in the context of steatotic liver.

In conclusion, the present study revealed that Orm1 is a protective factor against steatotic hepatic I/R. Orm1 is upregulated upon I/R; its loss aggravates hepatocellular damage and apoptosis, whereas its overexpression confers protection. Mechanistically, Orm1 binds Prdx1 to shield it from ubiquitin-proteasome degradation, thereby activating Pi3k/Akt survival signalling. Collectively, our findings establish the Orm1-Prdx1-Pi3k/Akt cascade as a promising therapeutic axis for steatotic liver I/R.

Acknowledgements

The authors acknowledge Dr Jijun Shan at Nanjing University Drum Tower Hospital for his invaluable guidance on the research ideas provided to the student Yuming Wang in the present study.

Funding

The present study was supported by the National Natural Science Foundation of China (grant nos. 82370666 and 82500972), Shandong Provincial Natural Science Foundation (grant no. ZR2025QC1668) and Qingdao Natural Science Foundation (grant no. 25-1-1-144-zyyd jch).

Availability of data and materials

The RNA sequencing data generated in the present study may be found in the National Genomics Data Centre under the accession number CRA048839 or at the following URL: https://ngdc.cncb.ac.cn/search/specific?db=bioproject&q=CRA048839). The IP-MS data generated in the present study may be found in the Integrated Proteome Resources (iProX) database under the accession number IPX0019637004 or at the following URL: https://www.iprox.cn//page/subproject.html?id=IPX0019637004). The other data generated in the present study may be requested from the corresponding author.

Authors' contributions

JC and XC designed the research and helped draft the manuscript. YuW, HC and RD performed the experiments. YuW, HL, RD, YiW and HC performed the statistical analyses. YiW and HC participated in data visualisation, including the generation of graphs and figures presented in the manuscript. JC and XC confirm the authenticity of all the raw data. All authors read and approved the final version of the manuscript.

Ethics approval and consent to participate

All animal experiments were conducted in accordance with the guidelines of the Animal Care and Use Committee of Qingdao University (ethics approval no. 20260401C57BL/64 520260601066).

Patient consent for publication

Not applicable.

Competing interests

The authors declare that they have no competing interests.

References

1. Lucey MR, Furuya KN and Foley DP: Liver transplantation. N Engl J Med 389: 1888-1900, 2023.
2. Song Z, Han H, Ge X, Das S, Desert R, Athavale D, Chen W, Komakula SSB, Lantvit D and Nieto N: Deficiency of neutrophil high-mobility group box-1 in liver transplant recipients exacerbates early allograft injury in mice. Hepatology 78: 771-786, 2023.
3. Li Y, Yang P, Ye J, Xu Q, Wu J and Wang Y: Updated mechanisms of MASLD pathogenesis. Lipids Health Dis 23: 117, 2024.
4. Steinberg GR, Valvano CM, De Nardo W and Watt MJ: Integrative metabolism in MASLD and MASH: Pathophysiology and emerging mechanisms. J Hepatol 83: 584-595, 2025.
5. Liu J, Pang L, Ng KTP, Chiu TLS, Liu H, Liu X, Xu A, Lo CM and Man K: Compromised AMPK-PGCIα axis exacerbated steatotic graft injury by dysregulating mitochondrial homeostasis in living donor liver transplantation. Ann Surg 276: e483-e492, 2022.
6. Liu R, Cao H, Zhang S, Cai M, Zou T, Wang G, Zhang D, Wang X, Xu J, Deng S, *et al*: ZBP1-mediated apoptosis and inflammation exacerbate steatotic liver ischemia/reperfusion injury. J Clin Invest 134: e180451, 2024.
7. Liu R, Wang G, Qian Y, Jiang Z, Wang W, Cai M, Zhang S, Wang G, Wang C, Zou T, *et al*: Hexosamine biosynthesis dysfunction-induced LIFR N-glycosylation deficiency exacerbates steatotic liver ischemia/reperfusion injury. Metabolism 168: 156258, 2025.
8. Sousa Da Silva RX, Bautista Borrego L, Lenggenhager D, Huwyler F, Binz J, Mancina L, Breuer E, Wernlé K, Hefti M, Mueller M, *et al*: Defatting of human livers during long-term e x situ normothermic perfusion: Novel strategy to rescue discarded organs for transplantation. Ann Surg 278: 669-675, 2023.
9. Sousa Da Silva RX, Weber A, Dutkowski P and Clavien PA: Machine perfusion in liver transplantation. Hepatology 76: 1531-1549, 2022.
10. Elmore S: Apoptosis: A review of programmed cell death. Toxicol Pathol 35: 495-516, 2007.
11. Xu X, Lai Y and Hua ZC: Apoptosis and apoptotic body: Disease message and therapeutic target potentials. Biosci Rep 39: BSR20180992, 2019.
12. de Oliveira THC and Gonçalves GKN: Liver ischemia reperfusion injury: Mechanisms, cellular pathways, and therapeutic approaches. Int Immunopharmacol 150: 114299, 2025.
13. Sahoo G, Samal D, Khandayataray P and Murthy MK: A review on caspases: Key regulators of biological activities and apoptosis. Mol Neurobiol 60: 5805-5837, 2023.
14. Beltrán-Visiedo M, Soler-Agesta R, Sarosiek KA, Green DR and Galluzzi L: Regulation of inflammatory processes by caspases. Nat Rev Mol Cell Biol 26: 884-901, 2025.
15. Budihardjo I, Oliver H, Lutter M, Luo X and Wang X: Biochemical pathways of caspase activation during apoptosis. Annu Rev Cell Dev Biol 15: 269-290, 1999.

16. Vogler M, Braun Y, Smith VM, Westhoff MA, Pereira RS, Pieper NM, Anders M, Callens M, Vervliet T, Abbas M, *et al*: The BCL2 family: From apoptosis mechanisms to new advances in targeted therapy. Signal Transduct Target Ther 10: 91, 2025.
17. Singh R, Letai A and Sarosiek K: Regulation of apoptosis in health and disease: The balancing act of BCL-2 family proteins. Nat Rev Mol Cell Biol 20: 175-193, 2019.
18. Sora V and Papaleo E: Structural details of BH3 motifs and BH3-mediated interactions: An updated perspective. Front Mol Biosci 9: 864874, 2022.
19. Yu G, Gao J, Hu W, Hu D, Wang W, Yang S and Gao J: ORM1 promotes tumor progression of kidney renal clear cell carcinoma (KIRC) through CALR-mediated apoptosis. Sci Rep 13: 15687, 2023.
20. Chen J, Zou L, Liu L, Wu C and Hu M: ORM1 mediates Ln-IgG-induced podocyte damage and autophagy via the AMPK/mTOR signaling. Organogenesis 21: 2519614, 2025.
21. Cheng X, Liu D, Xing R, Song H, Tian X, Yan C and Han Y: Orosomucoid 1 attenuates doxorubicin-induced oxidative stress and apoptosis in cardiomyocytes via Nrf2 signaling. Biomed Res Int 2020: 5923572, 2020.
22. Chen X, Liu Y, Mu S, Chen T, Yuan J, Xiao C, Dong Q, Li Q, Wang Y, Chen Q, *et al*: Orosomucoid 1 participates in alveolar hypercoagulation and fibrinolytic inhibition involving NF-κB signaling pathway in LPS-induced ARDS. FASEB J 39: e71147, 2025.
23. Fan C: Orosomucoid types in allergic contact dermatitis. Hum Hered 45: 117-120, 1995.
24. Astrup LB, Skovgaard K, Rasmussen RS, Iburg TM, Agerholm JS, Aalbæk B, Jensen HE, Nielsen OL, Johansen FF, Heegaard PMH and Leifsson PS: Staphylococcus aureus infected embolic stroke upregulates Orm1 and Cxcl2 in a rat model of septic stroke pathology. Neurol Res 41: 399-412, 2019.
25. Wu D, Xu J, Zhang Y, Wang Y, Bai Y, Zhan X, Gao Y, Zhou H, Hu H, Wang P and Rao Z: tBHQ mitigates fatty liver ischemia-reperfusion injury by activating Nrf2 to attenuate hepatocyte mitochondrial damage and macrophage STING activation. Int Immunopharmacol 138: 112515, 2024.
26. Livak KJ and Schmittgen TD: Analysis of relative gene expression data using real-time quantitative PCR and the 2(-Delta Delta C(T)) method. Methods 25: 402-408, 2001.
27. Yang X, Lu D, Wang R, Lian Z, Lin Z, Zhuo J, Chen H, Yang M, Tan W, Yang M, *et al*: Single-cell profiling reveals distinct immune phenotypes that contribute to ischaemia-reperfusion injury after steatotic liver transplantation. Cell Prolif 54: e13116, 2021.
28. Wu Y, Li C, Lu D, Chen K, Su R, Xu S, Gao F, Lian Z, Yang F, Chen J, *et al*: Insulin-induced gene 2 alleviates ischemia-reperfusion injury in steatotic liver by inhibiting GPX4-dependent ferroptosis. Cell Death Discov 11: 127, 2025.
29. Luo Z, Lei H, Sun Y, Liu X and Su DF: Orosomucoid, an acute response protein with multiple modulating activities. J Physiol Biochem 71: 329-340, 2015.
30. Patrono D, De Stefano N, Vissio E, Apostu AL, Petronio N, Vitelli G, Catalano G, Rizza G, Catalano S, Colli F, *et al*: How to preserve steatotic liver grafts for transplantation. J Clin Med 12: 3982, 2023.
31. Liu H and Man K: New insights in mechanisms and therapeutics for short- and long-term impacts of hepatic ischemia reperfusion injury post liver transplantation. Int J Mol Sci 22: 8210, 2021.
32. Xue X, Huang C, Chen J, Ding W, Ren Y, Zhang W, Li Q, Yang Z and Sun Z: Ginsenoside Rg1 mitigates sepsis-associated acute respiratory distress syndrome by promoting autophagy through the Prdx1-PTEN/PI3K/AKT pathway. Phytomedicine 154: 158027, 2026.
33. Zhang T, Li L, Mo X, Xie S, Liu S, Zhao N, Zhang H, Chen S, Zeng X, Wang S, *et al*: Matairesinol blunts adverse cardiac remodeling and heart failure induced by pressure overload by regulating Prdx1 and PI3K/AKT/FOXO1 signaling. Phytomedicine 135: 156054, 2024.
34. Xiong Y, Zhao X, Qin X, Zhang Y, Wang L, Zheng Q, Liu X, Liu H and Chen Z: OTUD7B attenuates renal fibrosis by regulating PRDX1 protein stability. J Adv Res: Mar 5, 2026 (Epub ahead of print). doi: 10.1016/j.jare.2026.02.059.
35. Sun X, Wu T, Chen S, Zhao Z, Jia R, Ma J, Yin L, Pan X, Ping Y, Mao Y, *et al*: OTUD1 inhibits osteoclast differentiation and osteoclastic bone loss through deubiquitinating and stabilizing PRDX1. Theranostics 15: 6719-6736, 2025.
36. Zhang Y, Wang Z, Jia C, Yu W, Li X, Xia N, Nie H, Wikana LP, Chen M, Ni Y, *et al*: Blockade of hepatocyte PCSK9 ameliorates hepatic ischemia-reperfusion injury by promoting pink1-parkin-mediated mitophagy. Cell Mol Gastroenterol Hepatol 17: 149-169, 2024.
37. Fournier T, Medjoubi NN and Porquet D: Alpha-1-acid glycoprotein. Biochim Biophys Acta 1482: 157-171, 2000.
38. Qiong L and Yin J: Characterization of alpha-1-acid glycoprotein as a potential biomarker for breast cancer. Bioengineered 13: 5818-5826, 2022.
39. Yue L, Xu X, Dai S, Xu F, Zhao W, Gu J, Dai X and Qian X: Orosomucoid 1 promotes colorectal cancer progression and liver metastasis by affecting PI3K/AKT pathway and inducing macrophage M2 polarization. Sci Rep 13: 14092, 2023.
40. Liu Z and Pu X: Orosomucoid 1 interacts with S100A12 and activates ERK signalling to expedite the advancement of bladder cancer. Cell Adh Migr 19: 1-11, 2025.
41. Zhang D, Zhang Y, Xia S, Chen L, Shen P and Yang C: Orosomucoid 1 ameliorates temporomandibular joint osteoarthritis by maintaining cartilage homeostasis. Adv Sci (Weinh) 12: e00028, 2025.
42. Yan N, Xia Y, Zhang Y, Sawaswong V, Xu X, Saito Y, Nanduri R, Dai M, Aibara D, Krausz KW, *et al*: Hepatocyte CEBPA-ORM1 axis restricts alcohol-associated liver disease. Hepatology: Mar 9, 2026 (Epub ahead of print).
43. Elpek GO: Orosomucoid in liver diseases. World J Gastroenterol 27: 7739-7747, 2021.
44. Elias-Miró M, Jiménez-Castro MB, Rodés J and Peralta C: Current knowledge on oxidative stress in hepatic ischemia/reperfusion. Free Radic Res 47: 555-568, 2013.
45. Deng RM and Zhou J: The role of PI3K/AKT signaling pathway in myocardial ischemia-reperfusion injury. Int Immunopharmacol 123: 110714, 2023.
46. Li Y, Xia J, Jiang N, Xian Y, Ju H, Wei Y and Zhang X: Corin protects H_2O_2-induced apoptosis through PI3K/AKT and NF-κB pathway in cardiomyocytes. Biomed Pharmacother 97: 594-599, 2018.
47. Zhang B, Zeng M, Li B, Kan Y, Wang S, Cao B, Huang Y, Zheng X and Feng W: Arbutin attenuates LPS-induced acute kidney injury by inhibiting inflammation and apoptosis via the PI3K/Akt/Nrf2 pathway. Phytomedicine 82: 153466, 2021.
48. Han X, Liu X, Zhao X, Wang X, Sun Y, Qu C, Liang J and Yang B: Dapagliflozin ameliorates sepsis-induced heart injury by inhibiting cardiomyocyte apoptosis and electrical remodeling through the PI3K/Akt pathway. Eur J Pharmacol 955: 175930, 2023.
49. Moretton A, Kourtis S, Gañez Zapater A, Calabrò C, Espinar Calvo ML, Fontaine F, Darai E, Abad Cortel E, Block S, Pascual-Reguant L, *et al*: A metabolic map of the DNA damage response identifies PRDX1 in the control of nuclear ROS scavenging and aspartate availability. Mol Syst Biol 19: e11267, 2023.
50. Wang J, Zhang Y, Cao J, Wang Y, Anwar N, Zhang Z, Zhang D, Ma Y, Xiao Y, Xiao L and Wang X: The role of autophagy in bone metabolism and clinical significance. Autophagy 19: 2409-2427, 2023.
51. Li J, Sun Y, Zhao X, Ma Y, Xie Y, Liu S, Hui B, Shi X, Sun X and Zhang X: Radiation induces IRAK1 expression to promote radioresistance by suppressing autophagic cell death via decreasing the ubiquitination of PRDX1 in glioma cells. Cell Death Dis 14: 259, 2023.

Copyright © 2026 Wang et al. This work is licensed under a Creative Commons Attribution-NonCommercial-NoDerivatives 4.0 International (CC BY-NC-ND 4.0) License.